Effects of topography on simulated net primary productivity at landscape scale

X.F. Chen[a,b], J.M. Chen[c,*], S.Q. An[b], W.M. Ju[c]

[a]*International Institute of Earth System Science, Nanjing University, Nanjing 210093, China*
[b]*School of Life Science, Nanjing University, Nanjing 210093, China*
[c]*Department of Geography and Program in Planning, University of Toronto, 100 St. George St., Room 5047, Toronto, Ont., Canada M5S 3G3*

Abstract

Local topography significantly affects spatial variations of climatic variables and soil water movement in complex terrain. Therefore, the distribution and productivity of ecosystems are closely linked to topography. Using a coupled terrestrial carbon and hydrological model (BEPS-TerrainLab model), the topographic effects on the net primary productivity (NPP) are analyzed through four modelling experiments for a 5700 km^2 area in Baohe River basin, Shaanxi Province, northwest of China. The model was able to capture 81% of the variability in NPP estimated from tree rings, with a mean relative error of 3.1%. The average NPP in 2003 for the study area was 741 g C m^{-2} yr^{-1} from a model run including topographic effects on the distributions of climate variables and lateral flow of ground water. Topography has considerable effect on NPP, which peaks near 1350 m above the sea level. An elevation increase of 100 m above this level reduces the average annual NPP by about 25 g C m^{-2}. The terrain aspect gives rise to a NPP change of 5% for forests located below 1900 m as a result of its influence on incident solar radiation. For the whole study area, a simulation totally excluding topographic effects on the distributions of climatic variables and ground water movement overestimated the average NPP by 5%.
© 2006 Elsevier Ltd. All rights reserved.

Keywords: BEPS-terrain lab; Net primary productivity; Topography

1. Introduction

Terrestrial carbon (C) and water cycles are tightly linked at various temporal and spatial scales (Ball et al., 1987; Leuning, 1995; Rodriguez-Iturbe, 2000). Terrestrial carbon assimilation by vegetation is very sensitive to soil moisture content in the root zone due to the strong dependence of stomatal conductance on soil water conditions (Jarvis, 1976). The response of C assimilation to soil wetness depends on plant species (Grant et al., 2006). Multi-year eddy correlation measurements showed that net C exchange of deciduous forests was more sensitive to drought than that of coniferous forests (Kljun et al., 2004).

Reliable simulation of the net C exchange between terrestrial ecosystems and the atmosphere requires accurate modeling of soil moisture content. However, the simulation of soil moisture content is difficult owing to its dependence on many factors, such as vegetation, soil, climate and topography and due to its large temporal and spatial variations. The redistribution of water in soils is controlled by many topographic factors (Qiu et al., 2001) including slope (Moore et al., 1988), aspect (Western et al., 1999), curvatures (Western et al., 1999), and slope position and relative elevation (Grayson et al., 1997).

In recent decades, a great diversity of terrestrial ecosystem models has been developed for simulating C, nutrient, energy, and water cycles at global and regional scales (Sellers et al., 1986, 1996; Dickinson et al., 1986; Neilson and Marks, 1994; Neilson, 1995; Haxeltine and Prentice, 1996; Kucharik et al., 2000; Bonan et al., 2003). They adopted different strategies to calculate the vertical movement of water in soils and the water flux between terrestrial ecosystems and the atmosphere. However, few of these models consider the lateral movement of ground water, or they quantify this redistribution simply according

---

*Corresponding author. Tel.: +1 416 978 7085; fax: +1 416 946 3886.
E-mail address: chenj@geog.utoronto.ca (J.M. Chen).

to the local slope using one-directional flow algorithms (Beven and Kirkby, 1979; Sellers et al., 1986, 1996; Abramopoulos et al., 1988). This kind of simplification in simulating soil moisture content is at times questionable, especially in complex terrains with large elevation variability (Soulis et al., 2000), because it can cause underestimation of soil moisture content in water-convergent regions and overestimation of soil moisture content in water-divergent areas. Unrealistic simulations of soil moisture content would definitely give rise to biases in simulated net C exchange between ecosystems and the atmosphere. In addition to the role in the redistribution of soil water, topography also has remarkable effects on microclimate including temperature, precipitation and absorbed solar radiation (Wigmosta et al., 1994; Brown et al., 2003). In terrestrial modeling, all of these topographic effects must therefore be carefully described.

The main objectives of this study were: (1) to highlight the coupling strategies of the BEPS-TerrainLab model; (2) to analyze the spatial distribution patterns of simulated annual net primary productivity (NPP) of 2003 in a 5700 km² of Baohe River Basin, Shaanxi Province, northwest of China at 30 m resolution; and (3) to partition the topographic effects on NPP into contributions from changes in climate variables and in lateral movement of ground water.

2. Model description

The tool used for this research is the BEPS (Boreal Ecosystem Productivity Simulator)-TerrainLab model, which was developed to simulate spatially explicit C and water fluxes between terrestrial ecosystems and the atmosphere with the inclusion of topographic effects. The coupled model is driven by remotely sensed vegetation parameters (leaf area index (LAI), land cover type), climate, soil texture, and digital elevation model (DEM). BEPS was originally developed to simulate NPP of the boreal forests at daily time steps. It contains a canopy-level photosynthesis model developed from Farquhar's leaf-level biochemical model (Farquhar et al., 1980) using a temporal and spatial scaling scheme (Chen et al., 1999), and a bucket soil water model to simulate the variation of soil moisture content (Liu et al., 1999, 2002). The canopy is separated into sunlit and shaded leaves according to a foliage clumping index, LAI, and solar zenith angle (Chen et al., 1999). For each of the two leaf groups, daily photosynthesis and transpiration are calculated (Chen et al., 1999; Liu et al., 2002, 2003). The model has been used in different ecosystems with a proven ability to provide reliable estimates of NPP (Amiro et al., 2000; Matsushita and Tamura, 2002; Sun et al., 2004).

TerrainLab is a spatially distributed hydrological model, which was designed to provide realistic simulations of water table depth and soil moisture content for modelling C balance of terrestrial ecosystems. This model comprehensively describes topographic effects on the spatial

variations of climatic variables and the movement of soil water via a subsurface saturated flow mechanism. It separates the soil profile into unsaturated and saturated zones. Soil water can move between these layers through vertical percolation and capillary rise, which are calculated according to water table depth, soil moisture content in the unsaturated zone, and hydrological parameters derived from soil texture. The extraction of water for transpiration from the two layers is partitioned according to the relative abundance of active roots (Jackson et al., 1996). Each pixel is linked with its surrounding 8 pixels by saturated subsurface baseflow, which is computed according to local slope and water table. The methodology to compute this baseflow was mainly adapted from Wigmosta's model (Wigmosta et al., 1994). This model has been modified and validated in a forested watershed of Canada (Chen et al., 2005). Same as BEPS, TerrainLab is also operated at daily time steps.

The detailed formulations of BEPS and TerrainLab were introduced in previous publications (Liu et al., 1999, 2002, 2003; Chen et al., 1999, 2005). Here we only highlight their major characteristics and coupling strategy. The inputs to and outputs from the coupled model, and information flows inside it are schematically shown in Fig. 1. The BEPS module calculates photosynthesis, autotrophic respiration, evaporation from soil and intercepted water, transpiration from canopy, and partition between rainfall and snow. Calculated evaporation and transpiration are transferred into the TerrainLab module for updating soil water balance in unsaturated and saturated zones. Simulated soil moisture content and water table depth in Terrainlab are used in the BEPS module to evaluate the effect of soil water on stomatal openness with Jarvis' method (Jarvis, 1976). Processes simulated in the coupled model (Fig. 2) include photosynthesis, autotrophic respiration, and transpiration from overstorey and understorey, evaporation from soil and intercepted water, and vertical as well as lateral movements of soil water. The major modification to BEPS after Chen et al. (2005) is the method for quantifying the effect of soil water on stomatal conductance. The modifier of soil water to stomatal conductance $f(\theta)$ is now computed as

$$f(\theta) = (1 - \beta^Z)f(\theta_u) + \beta^z 0.5, \tag{1}$$

where β is the fitted extinction coefficient; z is the thickness of the unsaturated zone (cm); θ_u is volumetric soil moisture content of the unsaturated zone; and the constant 0.5 in Eq. (1) means that the saturation of soil in the saturated zone reduces stomatal conductance by 50% (Chen et al., 2005). The value of $f(\theta_u)$ is computed as

$$f(\theta_u) = \begin{cases} 0, & \theta_u < \theta_{wp}, \\ \frac{\theta_u - \theta_{wp}}{\theta_{fc} - \theta_{wp}}, & \theta_{wp} < \theta_u < \theta_{fc}, \\ 1 - 0.5\frac{\theta_u - \theta_{fc}}{\theta_{sc} - \theta_{fc}}, & \theta_{fc} < \theta_u < \theta_{sc}, \end{cases} \tag{2}$$
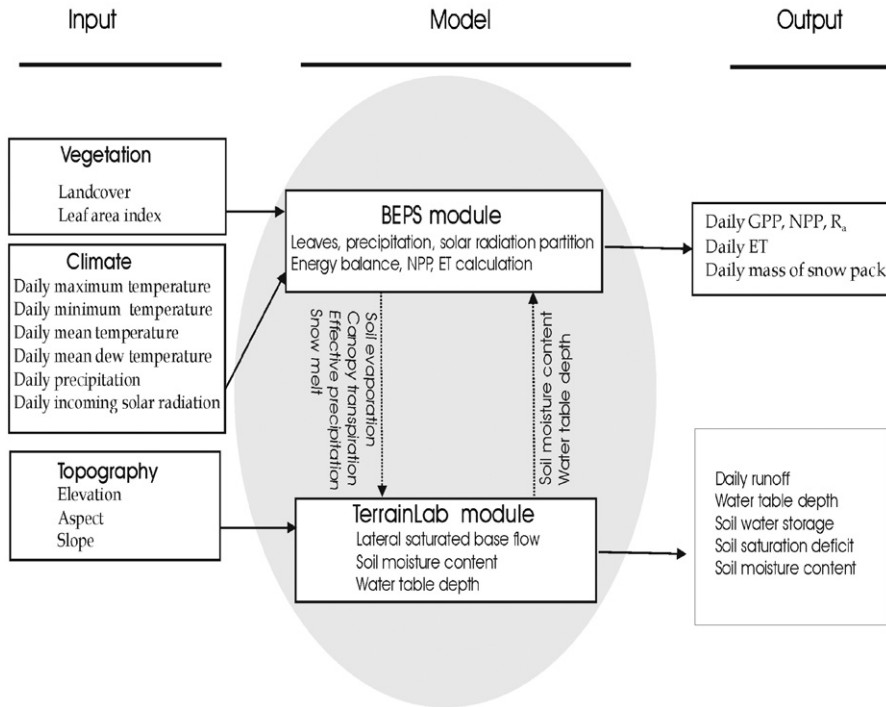
Fig. 1. The major components and interactions of the coupled BEPS-TerrianLab model. The soil moisture content is the key for the coupling of BEPS and TerrainLab modules and the calculation of NPP.
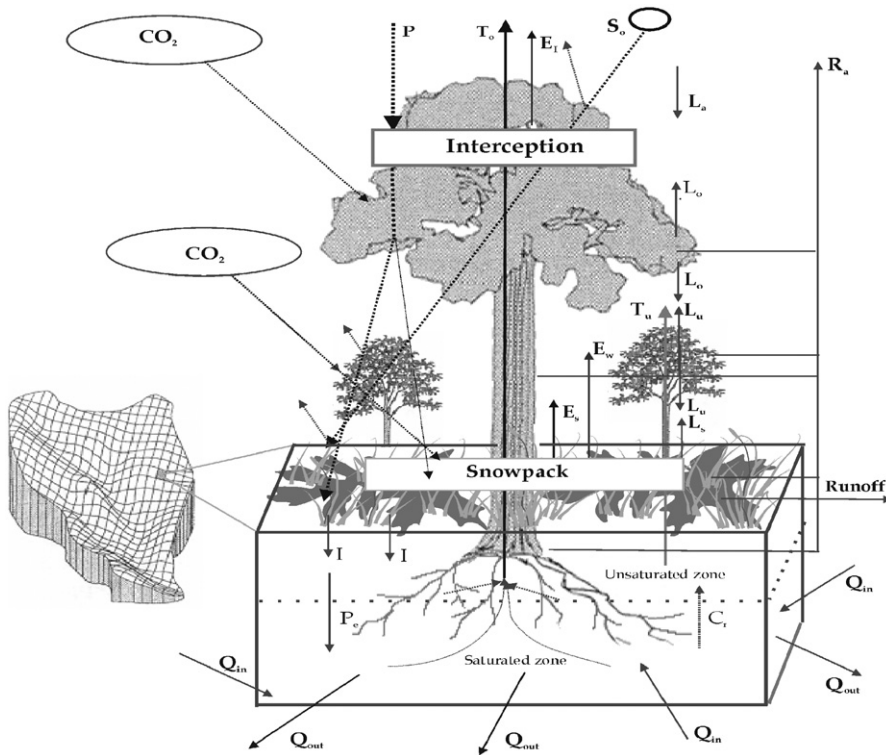
Fig. 2. Major processes described in the BEPS-TerrainLab model. Each pixel is interactively linked with 8 neighboring pixels via saturated subsurface baseflow. The exchanges of water and carbon between terrestrial ecosystems and the atmosphere are individually simulated for each pixel. Q_{in} and Q_{out} are saturated subsurface base inflow and outflow, respectively; P_e is the percolation from unsaturated zone to saturated zone; C_r is capillary rise. S_o is incoming solar radiation; E represents evaporation; T is transpiration and P is precipitation. Subscripts a, o, u and s represent air, overstorey, understorey and soil.

where θ_u is the volumetric soil moisture content in the unsaturated zone; θ_{wp} is the permanent wilting point; θ_{fc} is the field capacity; and $\theta_{sc}(z)$ is the volumetric soil water content at saturation. Parameters θ_{wp}, θ_{fc}, θ_{sc} are set following Kucharik et al. (2000).

3. Data used

Inputs to BEPS-TerrainLab include LAI and land cover type maps derived from remote sensing data, climate data interpolated from measurements at the reference weather station, DEM, and soil texture data. All data sets are processed into 30-m resolutions with a UTM projection.

3.1. Remote sensing data

Two Landsat TM images at 30 m resolution (path/row:128/36,128/37) were acquired on June 5, 2003, during the same period as the field experiment conducted in 2004. The two images were first geo-referenced using second-order polynomial transformation with ENVI software package. Ground control points were collected from 1:50,000 maps. Overall geo-referenced error was limited to less than 1 pixel (30 m). These two images were merged into one after geometric correction. The remote sensing map was masked according to the boundary of Baohe River Basin. Atmospheric corrections were carried out using the 6S code (Vermonte et al., 1997), which was parameterized assuming a middle latitude summer airmass and the atmospheric visibility of 30 km. After the atmospheric correction, the radiances of bands 3 and 4 were converted into reflectance for calculating Normalized Difference Vegetation Index (NDVI) and Simple Ratio (SR), from which a LAI map was produced (Chen et al., 2006). The remotely sensed LAI was compared with LAI measured using Tracing Radiation and Architecture of Canopies (TRAC; Chen, 1996) at 9 stands (two among the points have identical values) (Fig. 3). The remotely sensed LAI values presented here are the averages of 3 pixel × 3 pixel windows centered at the pixel where field LAI measurements were made. Remotely sensed LAI is in good agreement with field measurements ($R^2 = 0.77$). The LAI ranged from 0.5 to 5.0, most pixels having LAI = 4.0 (Fig. 4).

Land cover classification was implemented using the maximum likelihood supervised classification algorithm. Training samples were collected from a detailed field land cover map (forestry inventroy map). We classified the land cover of Baohe River Basin into three types, i.e., coniferous forest, mixed forest, and open land. The classification accuracy assessment resulted in the Kappa value of 72%.

3.2. Measured LAI and NPP data

LAI was measured at 9 sampling plots using the TRAC instrument in June, 2004, and tree rings were taken at the same time. The area of each sampling plot is about
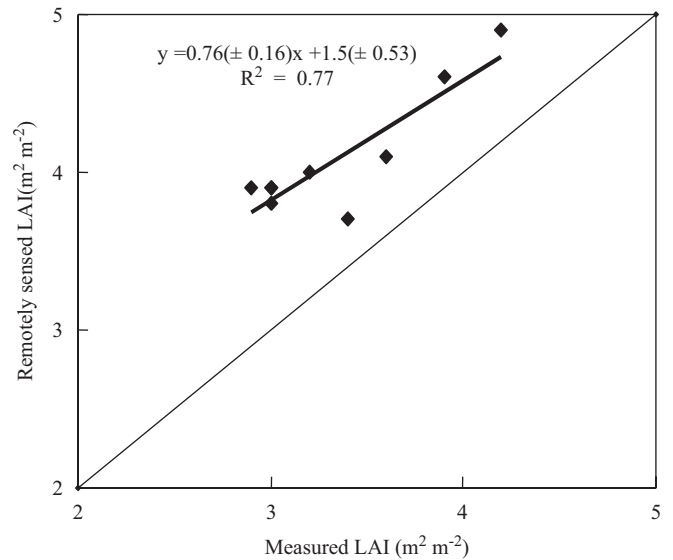

Fig. 3. LAI derived from remote sensing data compared with LAI measured with TRAC at 9 plots. The LAI from remote sensing is the average of LAI values in 3 pixel × 3 pixel windows centered at the pixel where ground LAI was measured using TRAC. The solid line is the 1:1 line. The values in the brackets of the regression equation are standard errors.
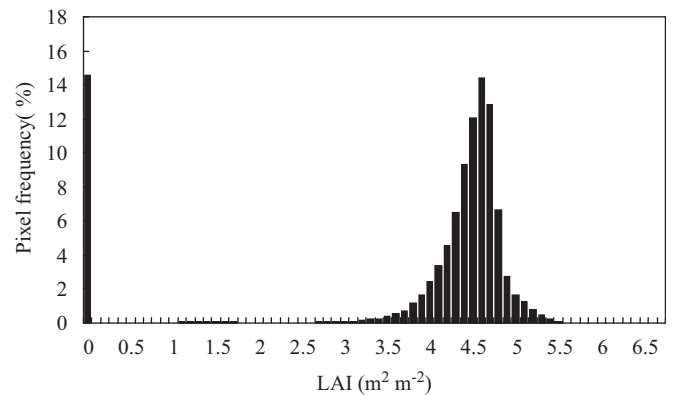

Fig. 4. Histogram of LAI in 2003.

30 m × 30 m, equal to the grid size of the Landsat TM data. Auxiliary data such as geographic coordinates were obtained using a Magellan global positioning system (GPS) with an accuracy of 5 m. LAI was calculated according to the measured canopy gap fraction after taking into account the element clumping index derived from the gap size distribution.

The following stand variables were measured: bark thickness and diameter at 1.3 m breast height (DBH), tree height, height to crown base (using a Vertex hypsometer), and crown radius (estimated from beneath the canopy). DBH, measured in perpendicular directions, and bark thicknesses, measured in opposite directions, had a precision of 1 mm. The heights and the crown width were measured with a precision of 10 cm. Tree-ring samples were collected with a 5-mm incremental borer applied at DBH

(1.3 m). The cores were immediately glued onto wooden mounts and surfaced with a series of successively finer sandpaper grits. Tree-ring series were dated following standard procedure (Stokes and Smiley, 1968). At least 9 dominant trees were cored at each site in plots with no evidence of tree mortality. Two cores (one from the north and one from the south) were taken at the breast height for each tree. In total, 162 tree cores were collected. Tree age ranged from 24 to 58 years.

We adopted the relative growth method to measure the biomass (Feng and Wu, 1999). The biomass of each component (stem, branch, leaf, root) was estimated from the tree height and the DBH using formulae derived from the field measurements (Table 1). The increments of DBH were obtained from the tree ring samples, which were then used to estimate the increment of each biomass component for each tree from 2002 to 2003. The annual NPP of a sampling plot was calculated from the number of trees in each plot, and from the change of biomass between 2 years, which was in turn estimated from the increment of DBH.

In this study area, a good relationship was found between measured LAI and inventory NPP (Fig. 5). Overall, the annual NPP increased by $206 \, \mathrm{g \, C \, m^{-2} \, yr^{-1}}$ per unit LAI. This NPP data from inventory will be used for model validation, which is discussed below.

3.3. Soil data

A soil map (at 1:250,000 scale) was digitized using ARC/INFO. This vector soil map was then rasterized to produce maps of sand, clay and silt fractions. These maps were used to determine hydrological parameters, including the wilting point, field capacity, porosity, an exponent of the moisture release equation, saturated hydraulic conductivity at the ground surface, and air entry water potential (Campbell and Norman, 1998). All hydrological parameters are assumed vertically homogeneous in the soil profile except the saturated hydraulic conductivity, which is assumed to decrease with depth from the surface. The decay rate of saturated hydraulic conductivity with depth was assigned according to Beven (1997) and Coles et al. (1997).

3.4. DEM data

A 30-m resolution DEM dataset was used to derive the slope, aspect and wetness index. The derived slope and aspect maps were used in the interpolation of incoming radiation (Section 3.5). The wetness index map was used to initialize water table depth (Chen et al., 2005). The DEM data were also used in interpolating air temperature and calculating saturated subsurface lateral baseflow (Wigmosta et al., 1994; Chen et al., 2005).
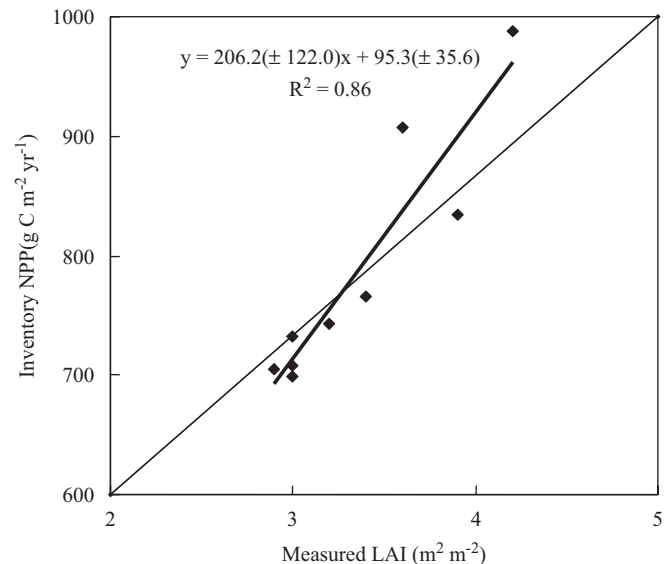

Fig. 5. Relationship between measured (inventory) NPP and LAI. NPP was calculated from the increment of tree rings, and LAI was measured using TRAC in 2004. The solid line is the 1:1 line. The values in the brackets of the regression equation are standard errors.

Table 1
Regression parameters of biomass and $D^2 H$

Species	Organ	Regression equation	r
Pinus armandi Franch	Stem	$W_b = 0.013 \, (D^2 H)^{1.0}$	0.92
	Branch	$W_s = 0.005 \, (D^2 H)^{1.0}$	0.91
	Leaf	$W_l = 0.001 \, (D^2 H)^{1.1}$	0.93
	Root	$W_r = 0.003 \, (D^2 H)^{1.0}$	0.93
Pinus tabulaeformis Carr	Stem	$\ln W_s = 0.99 \ln (D^2 H) - 10.49$	0.98
	Branch	$\ln W_b = 0.98 \ln (D^2 H) - 11.60$	0.98
	Leaf	$\ln W_l = 0.98 \ln (D^2 H) - 12.29$	0.95
	Root	$\ln W_r = 0.98 \ln (D^2 H) - 11.65$	0.89
Quercus spp	Stem	$\ln W_s = 0.85 \ln (D^2 H) - 3.00$	0.98
	Branch	$\ln W_b = 3.09 \ln (D^2 H) - 5.31$	0.90
	Leaf	$\ln W_l = 2.17 \ln (D^2 H) - 3.98$	0.90
	Root	$\ln W_r = 1.79 \ln (D^2 H) - 1.93$	0.90

3.5. Climate data

Climatic inputs required to run the model include daily maximum, minimum, mean and dew point temperatures, daily precipitation, and incoming solar radiation. All these climatic inputs are interpolated from measurements or derived values at the Baohe weather station. Solar radiation is not measured at this station. Daily values of this variable were calculated from daily amplitude of air temperature, precipitation, and water vapor pressure (Thornton and Running, 1999). All climatic variables were interpolated at 30 m resolution. In the interpolation, the horizontal spatial variability of climatic variables was not considered. The topographic effects on local microclimate were considered as follows. The vertical variations of temperature were corrected according to the difference in elevation between the weather station and the pixel processed. The lapse rates were set as 8 °C/km for maximum temperature and 1.25 °C/km for minimum and dew point temperatures (Running and Coughlan, 1988). The effect of aspect on temperatures and that of elevation on precipitation have not been taken into account. Since topography has different effects on the direct and diffuse components of incoming solar radiation (Wang et al., 2002), the direct component is corrected as (Wigmosta et al., 1994):

$$R_i = R_0 \frac{\cos \theta_c}{\cos \theta},\qquad(3)$$

where R_i is the solar radiation for the ith pixel; R_0 is the estimated solar radiation at the reference weather station; θ_c is the angle between the normal to the slope and sun–earth vector; θ is solar zenith angle. θ_c is determined by

$$\cos \theta_c = \cos \beta \cos \theta + \sin \beta \sin \theta \cos(\psi - \gamma),\qquad(4)$$

where β and γ are the terrain surface slope and aspect (North zero, increasing clockwise), respectively; ψ is the solar azimuth angle (North zero, increasing clockwise).

Topography has very small influences on diffuse radiation (Wang et al., 2002), as the reflected radiation from the surrounding terrain would more or less compensate for the reduction of diffuse radiation from the sky at sloping surfaces. For simplicity, we did not implement the correction for diffuse solar radiation. All pixels at different aspects receive the same amount of diffuse solar radiation, which was partitioned from the total using the ratio of global radiation to the solar irradiance above the atmosphere at the same latitude (Chen et al., 1999).

4. Site description and experimental design

4.1. Experimental site

The experimental site is located in the southwest slope of the Taibaishan Natural Reserve, at the middle of Qinling Mountains, which is an important mountain range affecting the climate of interior China and nearby areas in the southwest of Shaanxi Province (31°42′N–39°35′N, 105°29′E–110°15′E) (Fig. 6). The site has an elevation range from 518 to 3767 m above the sea level and a transition mountainous climate of a warm temperate and northern sub-tropic region. The annual rainfall is about 630 mm at low elevations and increases to about 1000 mm at the top of the Taibaishan Mountain. The mean annual air temperature decreases from +9.5 °C at the foot of the mountain to −4.5 °C at the top. Influenced by topography, the Qinling Mountains have clearly different vegetation covers in different terrain aspects, including pine (*Pinus armandi* Franch) and broadleaf mixed forest at elevations
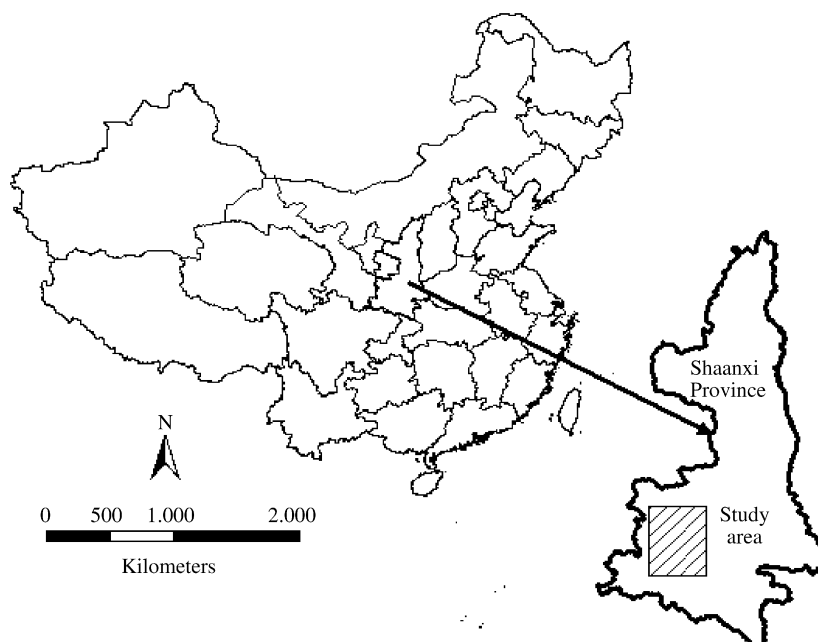

Fig. 6. Location of study area.

from 1330 to 3420 m in the northwest aspect, conifer (*Abies fabric* (Mast.) Graib., *Pinus tabulaeformis* Carr.) and broadleaf mixed forest at elevations from 734 to 1300 m in the north aspect, conifer forest in the alpine zone at elevations from 1250 to 3400 m in the west aspect, and pine (*Pinus armandi* Franch) and broadleaf mixed forest (*Quercus* spp) at elevations from 912 to 2428 m in the south aspect. The pine and broadleaf mixed forest is the dominant vegetation type. Vegetation density varies with elevation, providing a large natural setting for developing remote sensing algorithms of biophysical parameters. It is therefore also ideal for validating NPP models.

4.2. Experimental design

We designed a series of four simulation experiments in this study to investigate the importance of taking topographic effects into account in modelling NPP at the landscape scale (Table 2). In experiment I, we attempted to represent all topographic effects on ecological processes by considering the variations in climate variables with topography and the lateral movement of ground water related to the local gradient. In experiment II, we only considered the topographic influences on climate variables, and each pixel was isolated from surrounding pixels in simulating ground and soil water balance. This model run was to analyze the bias in the simulation of NPP due to unrealistic description of ground water movement in the mountainous areas. In experiment III, we only considered the subsurface lateral flow of soil water in calculating soil water balance. The climatic variables were not allowed to change with elevation and slope. In experiment IV, we treated the landscape as totally flat at the elevation of the weather station. The topographic effects on temperature, precipitation and solar radiation were excluded in the interpolations of these climatic variables. There was also no hydrological connection between a pixel and its neighbors. Soil water could move only vertically in the profile.

5. Results and discussion

5.1. Validation of simulated net primary productivity (NPP)

Simulated annual NPP values from different experiments were compared with those measured at 9 stands where LAI and tree ring measurements were taken. As expected, experiment I achieved the best agreement with measured NPP. The departure of modeled NPP from measured values was largest in experiment IV, implying the importance of considering topographic effects on NPP simulations (Table 3). With the consideration of topographic effects on climate and on lateral soil water redistribution, this model performed well in simulating the annual NPP for these sampled stands. It accounted for 81% of the variability in NPP across the sites, with a mean

relative error of 3.1% and the largest relative error of 10.1% (Fig. 7, Table 4). The model seems to overestimate NPP slightly at low productive sites but for stands with high productivity, the model produced slightly underestimated the annual NPP values in comparison with those from tree rings.

The discrepancy between model results and field measurements may be attributed to several reasons. First, the model differentiates only among land cover types, not among species. Second, the error in deriving LAI could also contribute to the discrepancy; for example, the topographic effects on remotely sensed reflectance were

Table 2
Design of four simulation experiments with different considerations of topographic effects on climate variables and the subsurface lateral flow of ground water

Experiment	Topographic effects on climate	Lateral flow of ground water
I	Yes	Yes
II	Yes	No
III	No	Yes
IV	No	No

Table 3
Correlation of measured NPP based on tree rings with modeled results for the four Experiments (The values in the brackets are standard error.)

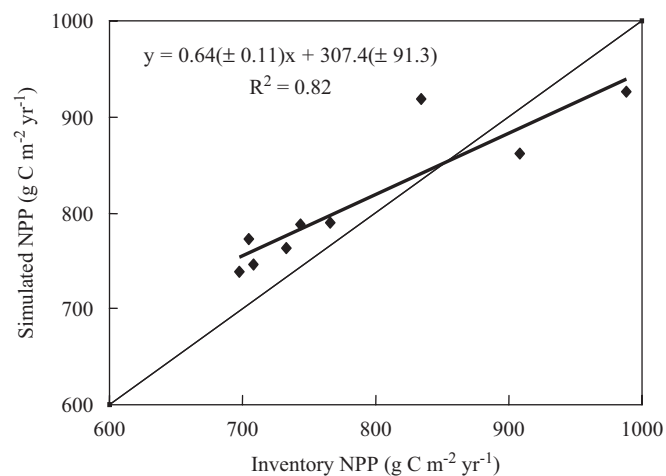| Experiment	Regression equation	R^2
I	$y = 0.64\,(\pm 0.11)x + 307.4\,(\pm 91.4)$	$R^2 = 0.82$
II	$y = 0.66\,(\pm 0.14)x + 277.7\,(\pm 111.4)$	$R^2 = 0.76$
III	$y = 0.47\,(\pm 0.12)x + 490.97\,(\pm 102.5)$	$R^2 = 0.65$
IV	$y = 0.46\,(\pm 0.13)x + 495.35\,(\pm 103.5)$	$R^2 = 0.64$

Fig. 7. Simulated NPP using BEPS-TerrainLab in comparison with (inventory) NPP calculated from tree ring data collected in the summer of 2004. The solid line is the 1:1 line. The values in the brackets of the regression equation are standard errors.

Table 4
Comparison between the modeled and measured NPP in 2003

Site	Forest type	Inventory NPP ($g\,C\,m^{-2}\,yr^{-1}$)	Modeled NPP ($g\,C\,m^{-2}\,yr^{-1}$)	Relative error(%)
1	*Pinus armandi* Franch and deciduous broadleaf forest	708.7	746.2	5.3
2	*Quercus* spp *Pinus tabulaeformis* Carr.forest	907.9	861.6	−5.1
3	*Pinus tabulaeformis* Carr.forest and deciduous broadleaf forest	834.1	918.3	10.1
4	*Pinus armandi* Franch	765.9	790.4	3.2
5	*Quercus* spp *Pinus tabulaeformis* Carr.forest	698.1	737.9	5.7
6	*Quercus* spp *Pinus tabulaeformis* Carr.forest	988.0	926.8	−6.2
7	*Pinus armandi* Franch	743.6	786.8	5.8
8	*Quercus* spp *Pinus tabulaeformis* Carr.forest	705.1	772.1	9.5
9	*Quercus* spp *Pinus tabulaeformis* Carr.forest	732.6	762.6	4.1
Mean		787.1	811.4	3.1

Fig. 8. Histogram of simulated annual NPP in 2003.

Table 5
Sensitivity analysis of simulated NPP to LAI in different elevation ranges

Elevation (m)	NPP_{dec} (80% LAI)	NPP (100% LAI)	NPP_{inc} (120% LAI)
0–800	603.55 (0.85)	710.87	846.65 (1.19)
800–1000	638.73 (0.84)	756.34	896.03 (1.18)
1000–1200	653.01 (0.84)	777.73	918.87 (1.18)
1200–1400	660.22 (0.83)	791.04	934.95 (1.18)
1400–1600	657.35 (0.83)	791.91	936.88 (1.18)
1600–1800	643.44 (0.83)	779.18	921.59 (1.18)
1800–2000	626.61 (0.82)	762.04	901.15 (1.18)
2000–2200	600.94 (0.82)	732.28	867.5 0 (1.18)
2200–2400	562.64 (0.82)	686.19	815.09 (1.19)
2400–2600	509.30 (0.82)	622.21	741.68 (1.19)
2600–2800	426.64 (0.82)	521.23	622.92 (1.20)
2800–3000	363.04 (0.82)	444.04	532.08 (1.20)
3000–3200	323.89 (0.82)	396.16	475.35 (1.20)
3200–3400	241.35 (0.82)	295.59	355.76 (1.20)
3400–3600	105.96 (0.81)	130.49	158.06 (1.21)

(*Note*: The unit of NPP is $g\,C\,m^{-2}\,yr^{-1}$. 80% LAI and 120% LAI in the brackets mean simulated NPP with a decrease of LAI by 20% and an increase of LAI by 20%, respectively. 100% LAI means simulated NPP without LAI change. The values in the brackets are the ratio of NPP_{dec} to NPP and NPP_{inc} to NPP, respectively.)

not corrected. Third, NPP estimated from tree rings also has some errors (average relative error 5.7%).

5.2. Simulated distribution of annual net primary productivity

Simulated NPP values for 2003 in the study area ranged from 400 to 920 $g\,C\,m^{-2}\,yr^{-1}$, with an average of 741 $g\,C\,m^{-2}\,yr^{-1}$. Most forest areas have NPP values between 700 and 880 $g\,C\,m^{-2}\,yr^{-1}$ (Fig. 8). Overall, NPP values were normally distributed with a skew toward the low range because forests at high elevations have low NPP. The average annual NPP was 740 and 743 $g\,C\,m^{-2}$ for coniferous forest and mixed forest, respectively. The NPP difference is quite small, and partially due to the elevation distribution of the coniferous and mixed forests: coniferous forests are normally located at higher elevations. Sensitivity analysis was done by comparing simulated NPP values before and after a reduction of LAI by 20% and an increase of LAI by 20%. The uncertainties in simulated NPP related to LAI for different elevation ranges were evaluated through a similar sensitivity analysis. In general, NPP is slightly sensitive to LAI (Table 5). Spatially,

patches of NPP are quite distinct and NPP variation follows variations of elevation and aspect. NPP is higher on south slopes than on north slopes (Fig. 9). The spatial pattern of NPP distribution is consistent with that of LAI distribution (not shown).

5.3. Topographic effects on net primary productivity distribution

In order to investigate the dependence of NPP on topography, simulated NPP from experiment I was averaged over different elevation and aspect ranges. On the average, simulated NPP was significantly related to elevation for all aspects (Fig. 10). NPP increased with elevation at locations less than 1350 m above the sea level and then decreased at higher altitudes. This results from the interplay of physiological temperature optimum of
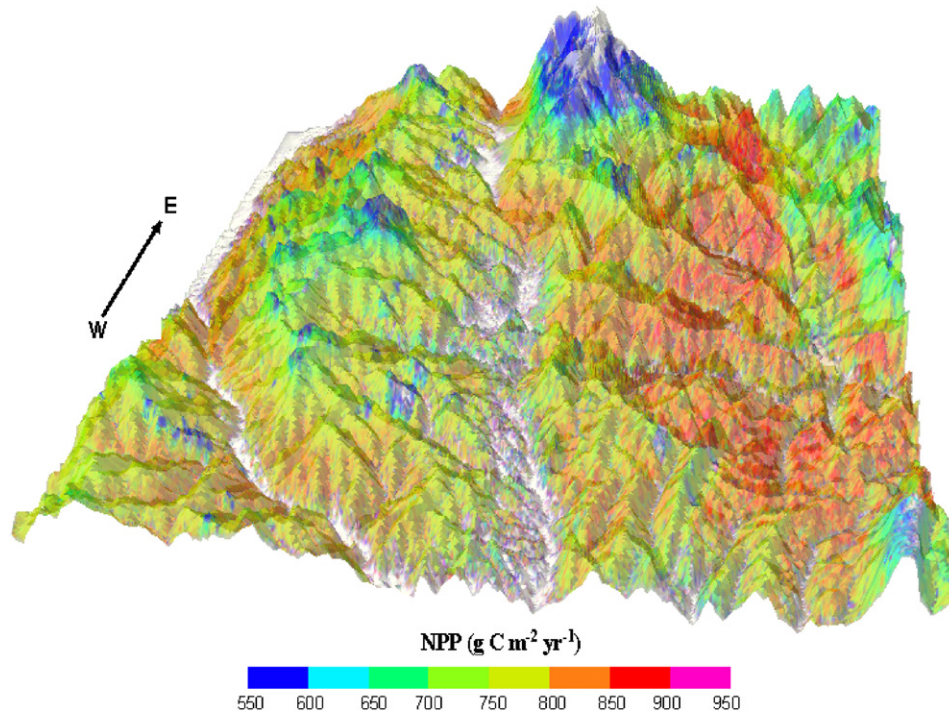
Fig. 9. Spatial distribution of simulated NPP in 2003. The areas in white color are bare soils.
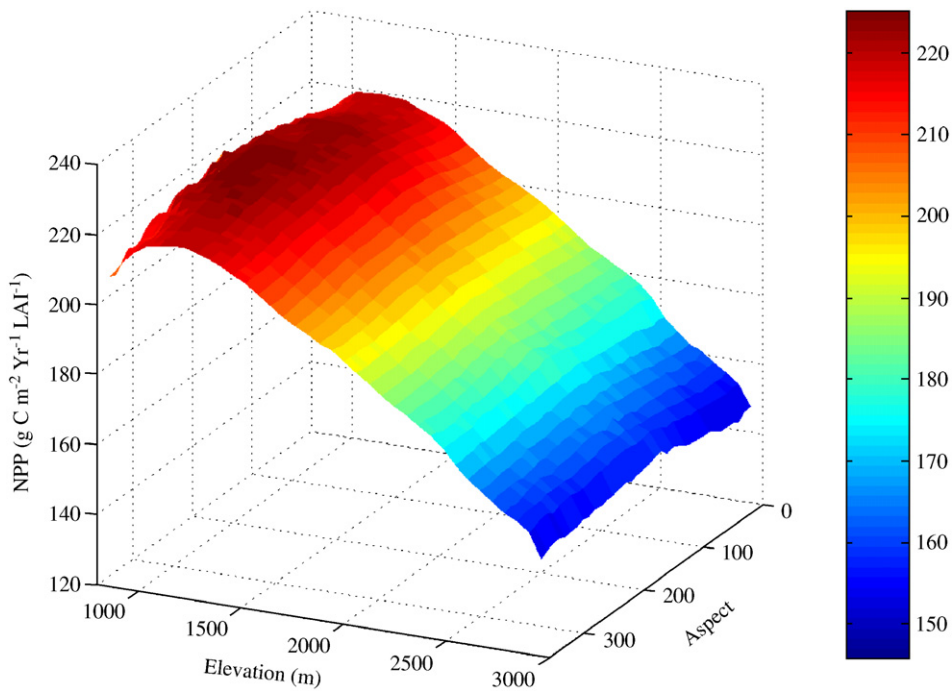

Fig. 10. The distribution of annual NPP per unit LAI (in $gC m^{-2} yr^{-1} LAI^{-1}$) varies with respect to elevation and aspect. Values shown here are the averages of NPP per unit LAI in different intervals of aspect and elevation. Aspect (in degree) is zero in the north and increases clockwise.

photosynthesis and altitudinal variation of temperatures (the lapse rates of daily maximum temperature are 8, and 1.25 °C/1000 m for minimum and dew point temperatures). At low elevations, summer daily mean temperatures were sometimes above the optimum temperature for photosynthesis (currently set in the model as 20 °C). The forest C

assimilation was at times limited by high temperature. In contrast, forests at high elevations experience temperatures below the optimum most of the time and therefore have low photosynthesis rates. For elevation above 1350 m, a 100 m increase in elevation results in a reduction of about 25 $gC m^{-2} yr^{-1}$ in average NPP. The average NPP of

forests above 3000 m is was only 50% of the peak value at the 1350 m height.

Aspect also plays an important role in determining the productivity of forests at elevations below 1900 m. In the study area, NPP increased from the north and peaked in the south following the pattern of direct solar radiation changes with aspect. In accordance with LAI, NPP approached the minimum at the northwest and then slightly increases again. The variation of NPP with aspect was generally below 6%. For elevations above 1900 m, the variation of NPP with aspect was irregular. At these locations, temperature seems a more important determinant of NPP than solar radiation. Therefore, aspect had smaller impact on NPP than elevation.

5.4. Sensitivity of simulated net primary productivity to topographic effects

The seasonality of simulated NPP from all experiments is shown in Table 6. The exclusion of both lateral saturated surface flow and topographic effects on interpolated climate data fields gave rise to the largest overestimation of NPP. Average NPP from experiment III (no topographic effects on interpolated climate fields) was higher than that from experiment II (no lateral redistribution of soil water). In experiment III, interpolated values of climate variables were spatially homogeneous, the limitation of low temperature on NPP at high elevations was unrealistically removed, and therefore NPP was overestimated. This experiment produced notably higher NPP values than did experiment I (fully integrated topographic effects) during months with low temperature. In summer, experiments I and III gave very similar NPP values. Annually, average NPP was about 3% higher in experiment III than in experiment I. With the consideration of lateral flow, canopy conductance was low in convergent and high in divergent locations of ground water. In divergent sites, soil water moves out through lateral subsurface flow and soil moisture is mostly below the field capacity whereas in convergent sites, soil water moves in and soil moisture is mostly above field capacity.

Table 6
Seasonality of simulated average NPP ($g\,C\,m^{-2}\,yr^{-1}$) in different experiments

Month	Experiment I	Experiment II	Experiment III	Experiment IV
Mar.	42.4	43.3	46.8	47.8
Apr.	81.1	82.8	84.6	86.4
May	104.3	106.4	107.3	109.4
Jun.	113.4	115.6	114.5	116.7
Jul.	113.0	115.3	114.1	116.4
Aug.	103.9	106.0	105.0	107.1
Sep.	87.6	89.3	90.0	91.9
Oct.	61.0	62.2	64.3	65.6
Nov.	34.1	34.8	37.7	38.5
Annual	740.7	755.7	764.3	779.8

The departure of soil water from the field capacity reduces canopy conductance and consequently NPP. Therefore, experiment II also overestimated NPP in comparison with experiment I. As expected, experiment IV, which treated the landscape as completely flat, produced the highest average NPP. The exclusion of topographic effects on variations of climate induced larger overestimation of NPP than exclusion of lateral subsurface flow (Table 6). We emphasize that the effect of lateral water flow was small because this area generally has sufficient rainfall; in drier areas, this effect is expected to be much larger.

6. Conclusion

The BEPS-TerrainLab model, which couples the BEPS model with a spatially distributed hydrological model TerrainLab, was applied to a forested watershed, Baohe River Basin in China. Based on model validation and modelling experiments, the following conclusions may be drawn:

(1) Based on field data and Landsat TM images, the coupled BEPS-TerrainLab model successfully simulated NPP in Baohe River Basin, China. The results show that the modeled NPP values that incorporate the effects of topography, are in good agreement with NPP values derived from tree ring data, with a mean relative error of 3.1%, the largest relative error of 10.1%, and R^2 equal to 0.81.

(2) In an area with large topographical variations dealt with in this study, forest productivity depends on topographic location (elevation and aspect). The exclusion of topographic effects on the variations of climate fields and ground water redistribution produced an overestimation of 5% in NPP on the average. The exclusion of the effects of elevation and aspect on the distribution of temperature and radiation produced a larger uncertainty in simulated NPP than the exclusion of lateral subsurface flow since this study area is relative wet and photosynthesis is seldom limited by soil water.

(3) Temperature–elevation interactions strongly affected NPP. NPP peaked at 1350 m above sea level on south-facing slopes. The departure of NPP from its peak value is related to the altitudinal temperature distribution. Below 1350 m, photosynthesis was sometimes reduced by temperatures exceeding 20 °C whereas above 1350 m, photosynthesis was often limited by temperatures below 20 °C. Above 1350 m, the average annual NPP decreased about $25\,g\,C\,m^{-2}\,yr^{-1}$ for every 100 m increase in altitude. The inclusion of topographic effects on climate fields affected mainly average NPP in months with low temperature. In summer, this inclusion had a negligible effect on the average NPP.

(4) Aspect is another determinant of NPP. However, its role was limited to locations below 1900 m above sea level. At these heights, the change of NPP with aspect

was about 6%. Above this level, temperature plays a more important role in controlling photosynthesis rate than does radiation, and NPP irregularly changes with aspect.

In this study, the effect of aspect on distributions of climate variables was not included, and topographic influence on remote sensing data was not corrected. In addition, the differences in species physiology, seasonal adaptation and elevational acclimation of vegetation to climate conditions were not considered. These issues might, to some degree, impact the values about the topographic effects of simulated NPP. They need to be considered in the future work.

Topographic variations of our study area are large in terms of the elevation range. The effects of topography on temperature and radiation were the main causes of NPP variations with topographical position, while the subsurface lateral water flow among pixels had only a relatively small effect on NPP in this relatively wet region. In other areas, the topographic effects on NPP would be different depending on the climate regime, and we expect that the lateral water flow would have larger effects on NPP than this case study. The treatment of landscape as a flat surface in ecological models is therefore generally problematic in areas with considerable topographical variations. Results of this study suggest that it should be indeed necessary and very important to consider the effects of topography in simulating net primary productivity at landscape and larger scales.

Acknowledgments

References

Abramopoulos, F., Rouseneweig, C., Choudhury, B., 1988. Improved ground hydrology calculation for global climate models (GCMs): Soil water movement and evapotranspiration. Journal of Climate 1, 921–941.

Amiro, B.D., Chen, J.M., Liu, J., 2000. Net primary productivity following forest fire for Canadian ecoregions. Canadian Journal of Forest Research 30, 939–947.

Ball, J.T., Woodrow, I.E., Berry, J.A., 1987. A model predicting stomatal conductnnance amd its contribution to the control of photosynthesis under different environmental conditions. In: Progress in Photosynthesis Research. Martinus Nijhoff Publishers, Dordrecht, pp. 221–224.

Beven, K., 1997. TOPMODEL: A Critique. Hydrological Processes 11, 1069–1085.

Beven, K.J., Kirkby, M.J., 1979. A physically based variable contributing model of basin hydrology. Hydrological Science Bulletin 24, 43–69.

Bonan, G.B., Levis, S., Sitch, S., Vertenstein, M., Oleson, K.W., 2003. A dynamic global vegetation model for use with climate models: concepts and description of simulated vegetation dynamics. Global Change Biology 9, 1543–1566.

Brown, R.D., Brausnett, B., Robinson, D., 2003. Gridded northern American monthly snow depth and snow water equivalent for GCM evaluation. Atmosphere-Ocean 41, 1–14.

Campbell, G.S., Norman, J.M., 1998. An Introduction to Environmental Biophysics. Springer, New York, pp. 1291–144.

Chen, J.M., 1996. Optically-based methods for measuring seasonal variation in leaf area index of boreal conifer forests. Agricultural and Forest Meteorology 80, 135–163.

Chen, J.M., Liu, J., Cihlar, J., Goulden, M.L., 1999. Daily canopy photosynthesis model through temporal and spatial scaling for remote sensing applications. Ecological Modelling 124, 99–119.

Chen, J.M., Chen, X.Y., Ju, W.M., Geng, X.Y., 2005. Distributed hydrological model for mapping evapotranspiration using remote sensing inputs. Journal of Hydrology 305, 15–39.

Chen, X.F., Chen, J.M., An, S.Q., Liu, Y.H., Fang, X.Q., Wang, S.M., 2006. Comparing the estimates of forest leaf area indices from Landsat TM data using different atmospheric correction models. Chinese Journal of Ecology 7, 769–773.

Coles, N.A., Sivapalan, M., Larsen, J.E., Linnet, P.E., Fahrner, C.K., 1997. Modelling runoff generation on small agricultural catchments: can real world runoff responses be captured? Hydrological Processes 11, 111–136.

Dickinson, R.E., Sellers, A.H., Kennedy, P.J., Wilson, M.F., 1986. Biosphere-atmosphere transfer scheme (BATS) for the NCAR community climate model. NCAR Tech. Note TN-275. National Center for Atmosphere Research, Boulder, Colorado, USA.

Farquhar, G.D., von Caemmerer, S., Berry, J.A., 1980. A biochemical model of photosynthetic CO2 assimilation in leaves of C_3 species. Planta 149, 78–90.

Feng, Z.W., Wang, X.K., Wu, G., 1999. Biomass and productivity of forest ecosystem in China. Sciences Press, Beijing, China.

Grant, R. F., Zhang, Y., Yuan., F., Wang, S., Gaumont-Guay, D., Hanson, P. J., Chen, J. M., Black, T. A., Barr, A., Baldocchi, D. D., Arain, A., 2006. Modelling water stress effects on CO_2 and energy exchange in temperate and boreal deciduous forests. Global Biogeochemical Cycles, accepted for publication.

Grayson, R.B., Western, A.W., Chiew, F.H.S., Bloschl, G., 1997. Preferred states in spatial soil moisture patterns: local and nonlocal controls. Water Resources Research 33, 2897–2908.

Haxeltine, A., Prentice, I.C., 1996. Biome3: an equilibrium terrestrial biosphere model based on ecophysiological constraints, resource availability, and competition among plant functional types. Global Biogeochemical Cycles 10, 693–709.

Jackson, R.B., Canadell, J., Ehleringer, J.R., Mooney, H.A., Sala, O.E., Schulze, E.D., 1996. A global analysis of root distributions for terrestrial biomes. Oecologia 108, 389–411.

Jarvis, P.G., 1976. Interpretation of variations in leaf water potential and stomatal conductance found in canopies in field. Philosophical Transactions of the Royal Society of London Series B-Biological Sciences 273, 593–610.

Kljun, N., Black, T.A., Griffis, T.J., Barr, A.G., Gaumont-Guay, D., Morgenstern, K., McCaughey, J.H., Nesic, Z., 2004. Net carbon exchange of three boreal forests during a drought. In: Proceedings of

the 26th Conference on Agricultural and Forest Meteorology, August 23–27. Vancouver, BC, Canada.

Kucharik, C.J., Foley, J.A., Delire, C., Fisher, V.A., Coe, M.T., Lenters, J.D., Young-Molling, C., Ramankutty, N., Norman, J.M., Gower, S.T., 2000. Testing the performance of a dynamic global ecosystem model: water balance, carbon balance, and vegetation structure. Global Biogeochemical Cycles 14, 795–825.

Leuning, R., 1995. A critical-appraisal of a combined stomatal-photosynthesis model for C-3 plants. Plant Cell and Environment 18, 339–355.

Liu, J., Chen, J.M., Cihlar, J., Chen, W., 1999. Net primary productivity distribution in the BOREAS region from a process model using satellite and surface data. Journal of Geophysical Research-Atmospheres 104, 27735–27754.

Liu, J., Chen, J.M., Cihlar, J., Chen, W., 2002. Net primary productivity mapped for Canada at 1-Km resolution. Global Ecology and Biogeography 11, 115–129.

Liu, J., Chen, J.M., Cihlar, J., 2003. Mapping evapotranspiration based on remote sensing: an application to Canada's landmass. Water Resources Research 39 (7), 1189–1194.

Matsushita, B., Tamura, M., 2002. Integrating remotely sensed data with an ecosystem model to estimate net primary productivity in East Asia. Remote Sensing of Environment 81, 58–66.

Moore, I.D., Burch, G.J., Mackenzie, D.H., 1988. Topographic effects on the distribution of surface soil-water and the location of ephemeral gullies. Transactions of the Asae 31, 1098–1107.

Neilson, R.P., Marks, D., 1994. A global perspective of regional vegetation and hydrologic sensitivities from climatic-change. Journal of Vegetation Science 5, 715–730.

Neilson, R.P., 1995. A model for predicting continental-scale vegetation distribution and water-balance. Ecological Applications 5, 362–385.

Qiu, Y., Fu, B.J., Wang, J., Chen, L.D., 2001. Spatial variability of soil moisture content and its relation to environmental indices in a semi-arid gully catchment of the Loess Plateau, China. Journal of Arid Environments 49, 723–750.

Rodriguez-Iturbe, I., 2000. Ecohydrology: a hydrologic perspective of climate-soil-vegetation dynamics. Water Resources Research 36, 3–9.

Running, S.W., Coughlan, J.C., 1988. A general model of forest ecosystem processes for regional applications. I. Hydrologic balance, canopy gas exchange and primary production processes. Ecol. Model. 42, 125–154.

Sellers, P.J., Mintz, Y., Sud, Y.C., Dalcher, A., 1986. A simple biosphere model (SiB) for use within general-circulation models. Journal of the Atmospheric Sciences 43, 505–531.

Sellers, P.J., Randall, D.A., Collatz, G.J., Berry, J.A., Field, C.B., Dazlich, D.A., Zhang, C., Collelo, G.D., Bounoua, L., 1996. A revised land surface parameterization (SiB2) for atmospheric gcms .1. Model formulation. Journal of Climate 9, 676–705.

Soulis, E.D., Snelgrove, K.R., Kouwen, N., Seglenieks, F., Verseghy, D.L., 2000. Towards closing the vertical water balance in Canadian atmospheric models: coupling of the land surface scheme class with the distributed hydrological model watflood. Atmosphere-Ocean 38, 251–269.

Stokes, M.A., Smiley, T.L., 1968. An introduction to tree-ring dating. University of Chicago Press, Chicago.

Sun, R., Chen, J.M., Zhu, Q.J., Zhou, Y.Y., Liu, J., Li, J.T., Liu, S.H., Yan, G.J., Tang, S.H., 2004. Spatial distribution of net primary productivity and evapotranspiration in Changbaishan Natural Reserve,China,using Landsat ETM+ data. Can. J. Remote Sensing 30 (5), 731–742.

Thornton, P.E., Running, S.W., 1999. An improved algorithm for estimating incident daily solar radiation from measurements of temperature, humidity, and precipitation. Agricultural and Forest Meteorology 93, 211–228.

Vermonte, E., Tanre′, D., Deuze′, J.L., Herman, M., Morcette, J.J., 1997. Second simulation of the satellite signal in the solar spectrum: an overview. IEEE Transactions on Geoscience and Remote Sensing 35, 675–686.

Wang, S., Chen, W.J., Cihlar, J., 2002. New calculation methods of diurnal distribution of solar radiation and its interception by canopy over complex terrain. Ecological Modelling 155, 191–204.

Western, A.W., Grayson, R.B., Bloschl, G., Willgoose, G.R., Mcmahon, T.A., 1999. Observed spatial organization of soil moisture and its relation to terrain indices. Water Resources Research 35, 797–810.

Wigmosta, M.S., Vail, L.W., Lettenmaier, D.P., 1994. A distributed hydrology-vegetation model for complex terrain. Water Resources Research 30, 1665–1679.